IOPscience iopscience.iop.org

Home Search Collections Journals About Contact us My IOPscience

Electron bonds and hyperfine electric field gradient in the $Sr_{1-x}Ba_xHfO_3$ family

This article has been downloaded from IOPscience. Please scroll down to see the full text article.

2005 J. Phys.: Condens. Matter 17 7717

(http://iopscience.iop.org/0953-8984/17/48/021)

View the table of contents for this issue, or go to the journal homepage for more

Download details:
IP Address: 129.252.86.83
The article was downloaded on 28/05/2010 at 06:54

Please note that terms and conditions apply.

INSTITUTE OF PHYSICS PUBLISHING JOURNAL OF PHYSICS: CONDENSED MATTER

J. Phys.: Condens. Matter **17** (2005) 7717–7729 doi:10.1088/0953-8984/17/48/021

Electron bonds and hyperfine electric field gradient in the $Sr_{1-x}Ba_xHfO_3$ family

A López-García and R E Alonso

Programa TENAES—Departamento de Física, Facultad de Ciencias Exactas, Universidad Nacional de La Plata, CC-67, 1900 La Plata, Argentina

Received 5 August 2005, in final form 19 October 2005
Published 11 November 2005
Online at stacks.iop.org/JPhysCM/17/7717

Abstract

The study by x-ray diffraction and perturbed angular correlation spectroscopy of $Sr_{1-x}Ba_xHfO_3$ compounds for $x = 0.12, 0.25, 0.5, 0.75$ and 0.88 is presented. The hyperfine parameters are analysed in terms of ionic radii, ionic or covalent bonds, and cation–oxygen distances. A simple explanation of the behaviour of these parameters with composition is provided.

1. Introduction

In perovskites the effect of partial substitution by homovalent or heterovalent cations is of current interest because the new compounds, namely $A_{1-x}A'_xM_{1-y}M'_yO_3$ with $0 < x, y < 1$, will in general improve the properties of simple AMO_3, as was observed for example in $PbZr_{1-y}Ti_yO_3$ (PZT) and $BaTi_{1-y}Hf_yO_3$ (BTH). In these cases the competition between M–O and M′–O bonds mainly determines the properties of these materials because there is a strong correlation between the cation radii and the shape of the oxygen octahedron. As x runs from 0 to 1, the crystalline structure is mainly determined by the most abundant oxide. For intermediate compositions different situations have been observed. If one of the perovskites is cubic at room temperature and the other has several lower symmetry structures above this temperature, the change of composition could have the same effect as the change of temperature. In this way, by varying x, different structures can be observed keeping the temperature constant. This effect was observed in $Sr_{1-x}Ba_xZrO_3$ but not in PZT and BTH [1–3].

The influence of composition and temperature on the structure, electrical properties and hyperfine interaction at M-sites of $BaTi_{1-x}Hf_xO_3$ for ($0 \leqslant X \leqslant 1$) has been reported [3, 4]. The aim was to determine the effect produced by cation substitution at the M-site due to the different ionic radius and electron configuration of the impurity cation. For Ti-rich oxides ($x \lesssim 0.20$) as the Hf concentration increases, the crystalline structures detected are different to those of $BaTiO_3$ and the transition temperatures decreases with x. For $x > 0.2$, the structure of all oxides has cubic symmetry at room temperature (RT) and the broadening of the dielectric constant increases [3]. The hyperfine studies revealed that the z-component of electric field gradient (EFG) tensor (V_{zz}) in the cubic phase has a maximum for $x \approx 0.5$ while the relative

 © 2005 IOP Publishing Ltd Printed in the UK

line broadening of the hyperfine interaction is widest as long as the Hf or Ti concentrations are high [4]. Using the simple point charge model and assuming charge polarization of vacancies and different charge states of M and M′ cations, the relative values of V_{zz} were reproduced. In contrast, the behaviour of the asymmetry parameter and the line width of the hyperfine interaction is still unclear [4].

To continue the study of mixed perovskites we are interested this time in analysing mixed oxides with AA′MO3 composition, in particular the $Sr_{1-x}Ba_xHfO_3$ (SBH) family. The simple oxides, $SrHfO_3$ (SH) and $BaHfO_3$ (BH), have very different properties. For example, BH has a cubic structure from room temperature to ∼1400 K. In contrast, SH displays three phase transitions in the same temperature range: orthorhombic $Pnma \rightarrow$ orthorhombic $Cmcm \rightarrow$ tetragonal $I4/mcm \rightarrow$ cubic $Pm\bar{3}m$ at transition temperatures $T_{C1} \approx 700$ K, $T_{C2} \approx 900$ K and $T_{C3} \approx 1400$ K, respectively. In this work, the phase transition at T_{C1} was classified as first order, and the other two as second order or continuous [5]. The hyperfine interaction that characterizes both oxides was also detected and has been determined to be different [6–8].

Because the ionic radius of Ba ($r_{Ba} \approx 1.35$ Å) is larger than the Sr ionic radius ($r_{Ba} \approx 1.13$ Å), the partial substitution of this cation by Ba will produce alterations in the crystalline and electronic structures. Thus, a competition between the Sr–O and Ba–O interactions is established, and changes of the properties can be produced by varying the composition of the mixed oxides.

In this contribution the crystalline structures determined by x-ray diffraction (XRD) and the electric hyperfine interaction measured by perturbed angular correlation (PAC) spectroscopy at $^{181}Hf/^{181}Ta$ probes in polycrystalline samples of $Sr_{1-x}Ba_xHfO_3$ for $x = 0.12$, 0.25, 0.50, 0.75 and 0.88 are studied. The choice and preparation of ^{181}Hf probes via neutron capture of ^{180}Hf guarantees the M-site location of the ^{181}Ta daughter in the lattice. Besides, the Ta octahedral ions coordinated to oxygen have been observed in Aurivillius type compounds. This opens the possibility of following the phase transitions at a well-defined lattice site. By measuring the temperature dependence of the EFG we also hoped to gain information about the electron distribution and the existence of defects because such structures often lead to additional contributions to the PAC spectra.

2. Sample preparation

Samples of $Sr_{1-x}Ba_xHfO_3$ were prepared for the first time by the high-temperature solid state reaction technique, mixing stoichiometric quantities of high-purity $SrCO_3$, $BaCO_3$ and HfO_2 to obtain compounds with compositions $x = 0.88$, 0.75, 0.50, 0.25 and 0.12. The mixtures were consecutively ground and heated at 773 and 1273 K for 24 h and finally at 1573 K for 3 h. The thermal evolution of the mixtures was controlled by XRD analysis at RT. The diffraction patterns for all compositions showed that the compounds were almost completely crystallized after the second heating at 1273 K.

The XRD patterns of the as-prepared samples were fitted using the Rietveld method and the lattice parameters were obtained.

For PAC spectroscopy the ^{181}Ta probe was produced by thermal neutron capture of ^{180}Hf already contained in the sample as one of the natural isotopes of hafnium. The samples were irradiated with a flux of about 2×10^{13} N cm^{-2} s^{-1} for 7 h at approximately 60 °C in order to obtain an activity of 300 μCi. The ^{181}Ta concentration obtained remains lower than 1 ppm. This extremely small impurity concentration is expected not to affect the properties of the pure material.

2.1. PAC spectroscopy

The angular correlation function of a gamma–gamma cascade $W(\vartheta, t)$ whose intermediate nuclear state has a electric quadrupole moment Q that interacts with a randomly oriented local electric field gradient tensor (EFG), is given by [9]

$$W(\vartheta, t) = 1 + A_{22}G_{22}(t)P_2(\cos\vartheta) + A_{44}G_{44}(t)P_4(\cos\vartheta) \tag{1}$$

where

$$G_{kk}(t) = \Sigma f_s G^s_{kk}(t). \tag{2}$$

In the last expression f_s is the fraction of perturbed nuclei at site s and G^s_{kk} is the perturbation factor corresponding to those nuclei at this site. The sum is over the number of available sites.

The intermediate nuclear state of the 133–482 keV gamma–gamma cascade in ^{181}Ta has spin $I = 5/2$, $A_{22} \gg A_{44}$ and nuclear quadrupole moment $Q = 2.35 \times 10^{-24}$ cm^2 [10].

The perturbation factor has the form

$$G_{22}(t) = \sigma_{2o} + \Sigma\sigma_{2n}\cos(\omega_n t)\exp(-\omega_n \delta t) \tag{3}$$

where the sum runs from $n = 1$ to 3 and the frequencies ω_n are related to the energy splitting produced by the electric quadrupole interaction. These frequencies are functions of the quadrupole frequency $\omega_q = e^2V_{zz}Q/[4I(2I-1)\hbar]$ and the asymmetry parameter $\eta = (V_{xx} - V_{yy})/V_{zz}$. In the last expressions, V_{zz} is the major principal axis component of the EFG tensor that fulfils with the other two components the equation $V_{xx} + V_{yy} + V_{zz} = 0$. The σ_{kn} coefficients are known functions that depend on η.

The attenuation in the oscillation amplitude introduced in the right-hand side of equation (3) through the relative line width δ parameter, takes into account the frequency distribution with Lorentzian shape around the central value ω_q [11]. This frequency distribution is included in order to simulate possible lattice distortions and random distribution of imperfections originated by the presence of impurities at A and B sites, oxygen vacancies and other uncontrolled defects [11]. In particular, the Ta^{5+} probe inside the oxygen octahedral adds an extra electron. This extra electron could interact with the randomly distributed lattice defects distorting the charge distribution at the probe's neighbourhood and contributing in this way to the EFG and also to the total line width.

3. Experimental setup and data fit

The time spectra were measured with a two CsF detector spectrometer storing coincidence data at 90°, 180° and 270°. The apparatus has a resolution time of ≈1ns for the gamma–gamma cascade of ^{181}Ta. The coincidence spectra were obtained after an accumulation time of 1 day or more for every temperature. The anisotropy versus delay time or spin precession curve is obtained by forming the ratio

$$A_{22}G_{22}(t) = 2[C(180, t) - C(90, t)]/[C(180, t) + 2C(90, t)] \tag{4}$$

where $C(90, t)$ and $C(180, t)$ are the true coincidence counting rates measured at time t with angles between detectors of 90° (or 270°) and 180°, respectively.

The determination of the hyperfine parameters ω_q, η and δ was carried out by performing least-square fits of equation (3) to the experimental data (equation (4)).

For the measurement of the angular correlation spectra as a function of temperature, from room temperature (RT) up to 1373 K and then back to RT, the samples were heated *in situ* in a furnace with a thermal stability better than 1 K.

Table 1. The crystal system, space group, corresponding lattice parameters and the mean lattice parameter assuming a pseudo-cubic phase for the different compositions. (Note: In the crystal system and space group column, the prefixes O, T and C stand for orthorhombic, tetragonal and cubic, respectively.)

Ba (%)	Crystal system and space group	**a** (Å)	**b** (Å)	**c** (Å)	⟨**a**⟩ (Å)
0	O-$Pbnm$	5.7516	5.7646	8.1344	4.0701
12	O-$Pbnm$	5.7939	5.8104	8.1892	4.1000
25	O-$Cmcm$	8.2239	8.2108	8.2329	4.1113
50	T-$I4/mcm$	5.8475		8.2900	4.1348
75	C-$Pm\bar{3}m$	4.1561			4.1561
88	C-$Pm\bar{3}m$	4.1662			4.1662
100	C-$Pm\bar{3}m$	4.1700			4.1700

4. Sample characterization

Using the Rietveld method structural refinements for each composition were performed, and the results of the XRD analysis at RT are shown in table 1.

For each oxide, the crystal system, the space group and the corresponding lattice constants **a**, **b**, **c** of the real lattice are shown. Thus, the sequence of crystalline structures at RT obtained by increasing the Ba concentration in $Sr_{1-x}Ba_xHfO_3$ oxides is similar to that observed by increasing the temperature in $SrHfO_3$.

For $x = 0.25$ the crystalline structure at RT was previously fitted with T-$I4/mcm$ [12]. However, on repeating the refinement process with the O-$Pnma$ or O-$Cmcm$ structures better results were obtained.

Also included in table 1 is the mean lattice constant ⟨**a**⟩ of an equivalent $Pm\bar{3}m$ pseudo-cubic structure. For low-symmetry structures this approximation can be done by assuming that $\langle \mathbf{a} \rangle^3 = V$ where V is the volume of the actual cell for the unit formula. The maximum value of the distortion ratio $\mathbf{c}'/\mathbf{a}'$ or $\mathbf{b}'/\mathbf{a}'$ where $\mathbf{a}'$, $\mathbf{b}'$ and $\mathbf{c}'$ are the lattice constant of the unit cell for all non-cubic oxides is less than 1.03, indicating that this approximation seems to be reasonable.

4.1. PAC results

In figure 1 the spin precession curves measured at RT and fitted with static, asymmetric and disordered EFG interactions acting on Ta probes for all compositions are shown.

The fitted hyperfine parameters corresponding to the first measurement at RT and the last one also at RT after the whole thermal treatment coincide. These results would indicate that no radiation damage is present in the irradiated samples (see figure 2).

4.1.1. $Sr_{0.88}Ba_{0.12}HfO_3$, $Sr_{0.75}Ba_{0.25}HfO_3$ and $Sr_{0.5}Ba_{0.5}HfO_3$. The PAC results for these compositions have already been published, and only the general trend of the hyperfine parameters and new aspects not considered before will be examined here. In figure 2 the temperature dependence of the quadrupole frequency ω_Q for these three compounds is shown.

$Sr_{0.88}Ba_{0.12}HfO_3$. In $SrHfO_3$ at RT the hyperfine parameters are $\omega_Q = 18.3_2$ Mrad s^{-1}, $\eta = 0.47_3$ and $\delta = 29_3\%$ [6], while in $Sr_{0.88}Ba_{0.12}HfO_3$ the corresponding values at the same temperature are 23.3_4 Mrad s^{-1}, 0.46_3 and $23_3\%$ [13]. The substitution of one Sr cation by Ba in one of the vertices of a pseudo-cubic cell produced an increase of about 27% in the value of ω_Q and consequently in V_{zz}.

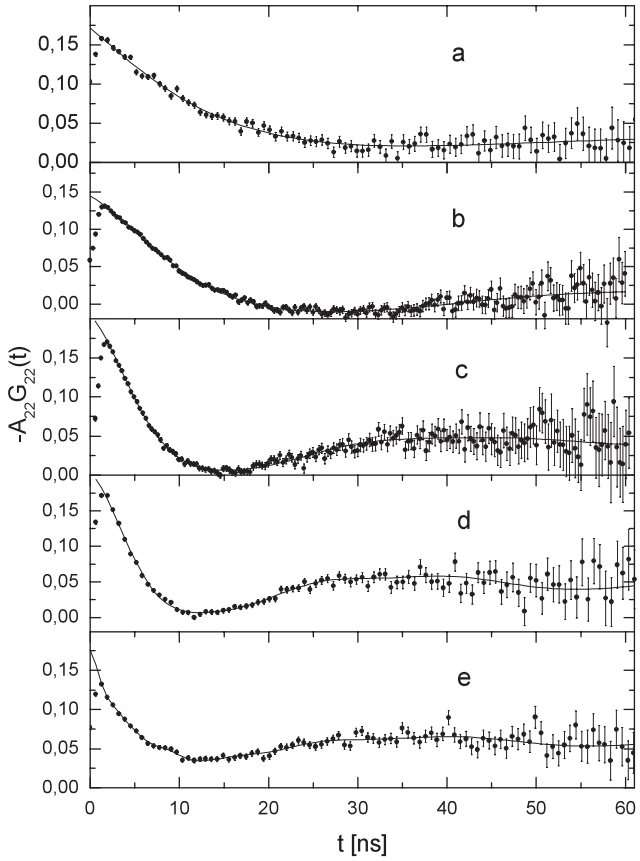

Figure 1. The experimental and fitted spin precession curves at RT: (a) $x = 0.88$, (b) $x = 0.75$, (c) $x = 0.5$, (d) $x = 0.25$ and (e) $x = 0.12$.

In addition, the asymmetry parameter has the same value for both oxides, indicating that the same change in V_{xx} and V_{yy} has occurred. Thus, the charge distribution originated by the substitution of one out of eight Sr cations by one Ba cation produced an EFG tensor whose diagonal components are proportional to those describing the EFG measured in $SrHfO_3$.

The value of δ measured in the pure sample ($29_3\%$) is similar to that found in $Sr_{0.88}Ba_{0.12}HfO_3$ ($23_3\%$), indicating that introducing this quantity of Ba would not produce any detectable change in the line width of the hyperfine interaction.

At about 500 K a discontinuous change in V_{zz} versus T is observed, exhibiting a first-order phase transition. Furthermore, two continuous phase transitions were also observed in the temperature dependence of the relative line width at ∼800 and ∼1000 K, respectively [13]. Thus in analogy to what was observed in $SrZrO_3$ (SZ) and $Sr_{1-x}Ba_xZrO_3$ (SBZ), and according to the crystallographic data of SH, these transitions would connect the following four structures as temperature increases: orthorhombic → orthorhombic → tetragonal → cubic.

$Sr_{0.75}Ba_{0.25}HfO_3$. In this composition Ba cations occupy two vertices of the pseudo-cubic cell. At RT the hyperfine parameters are $\omega_Q = 24.1_2$ Mrad s^{-1}, $\eta = 0.46_2$ and $\delta = 25_1\%$ [12]. Thus the duplication in the number of Ba ions produced a change in the crystalline structure, but the electronic structure at the Ta probe represented by the EFG seems to be not much affected as compared with those corresponding to the oxide with $x = 0.12$ [13].

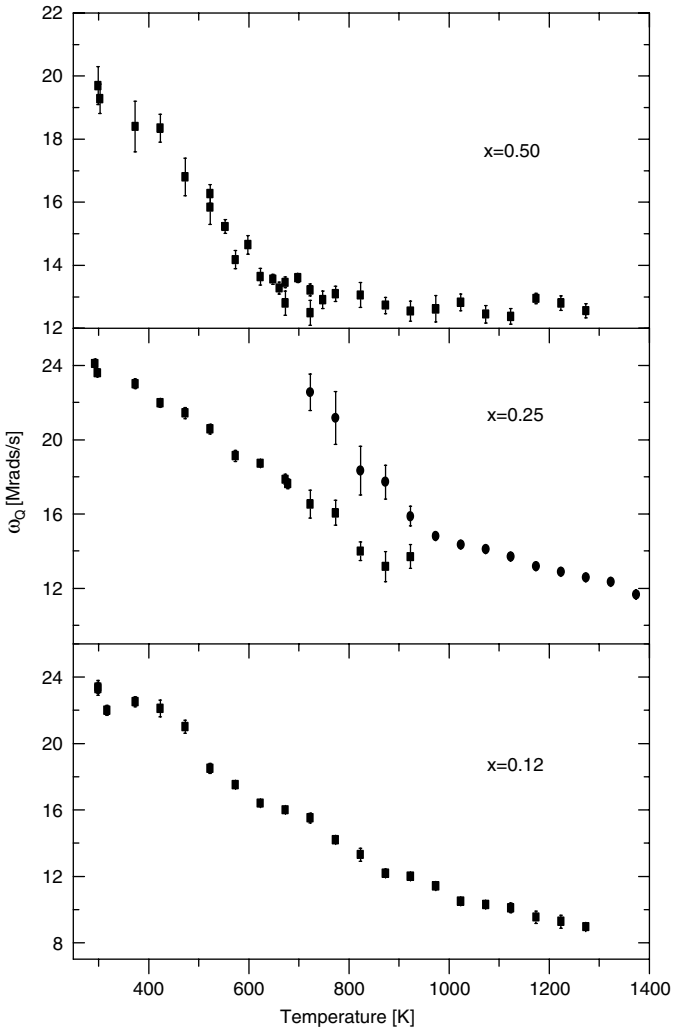

Figure 2. The quadrupole frequency versus temperature for $x = 0.12$, 0.25 and 0.50.

The phase transition from orthorhombic to cubic structure occurring between ∼700 and ∼950 K is of first order. In this temperature range two phases coexist. One of the phases corresponds to the low-temperature and the other to the high-temperature structure. The two-phase coexistence in the region of transformation temperatures could arise from different causes [14]. For example, in $BaTiO_3$ this coexistence was attributed to inhomogeneous distributions of nucleation sites probably located at point defects [15]. Another explanation for the two-phase coexistence was proposed for $LaCrO_3$ and $LaFeO_3$ oxides, and was based on the assumption that the local transformation temperature at each grain with different size is different [16]. There are still no reasons to adopt or reject either of these explanations or to assume that the embryos formed by thermal fluctuations are responsible. There are differences in the temperature dependence of the hyperfine parameters corresponding to these perovskites but the most relevant is the region of transformation temperatures: ∼250, ∼2, ∼18 and ∼30 K, respectively. A question arises: is it possible to assume a common mechanism that drives the phase transition in these cases or not?

Table 2. The hyperfine parameters fitted at RT for one-site and two-site models.

		Fraction	ω_Q (Mrad s^{-1})	η	δ (%)
1 site		100%	19.4 ± 0.5	0.45 ± 0.03	30 ± 3
2 sites	$I4/mcm$	84 ± 23	18.6 ± 0.8	0.43 ± 0.06	21 ± 8
	$Imma$	16 ± 4	16.5 ± 2.0	0 ± 0.1	2 ± 15

The temperature dependence of ω_Q corresponding to the cubic phase in the coexistence range has a different behaviour from that observed in the cubic structure above 950 K.

The line width is wider in the orthorhombic phase ($\delta \approx 25\%$) than in the cubic phase ($\delta \approx 18\%$). However, in the coexistence region when orthorhombic or cubic grains are small, δ in each phase is also small and increases with the grain size. This would indicate that in both phases as the grain size increases lattice distortions are incorporated.

The asymmetry parameter is almost temperature independent, except in the transition region where η is larger for the cubic structure.

$Sr_{0.50}Ba_{0.50}HfO_3$. In this composition there are an equal number of Sr and Ba cations at the vertices of the pseudo-cubic cell. In a recent work using high-resolution synchrotron XRD technique on a $Sr_{0.50}Ba_{0.50}HfO_3$ sample, Kennedy *et al* [17] reported a wide temperature region of two-phase coexistence: orthorhombic $Imma$ and tetragonal $I4/mcm$ from about 20 K up to RT.

At RT the fraction reported for the first phase is 62%. With this new information, our PAC data at RT were adjusted again using a model consisting of two static, asymmetric and disordered electric quadrupole interactions. The results of the new fit and the old one are shown in table 2.

In the two-site configuration the hyperfine parameters describing site 1 with $84_{23}\%$ abundance were assigned to the tetragonal structure and coincide within errors with those obtained by fitting the data with a unique site [18]. According to the diffraction studies, the other interaction would correspond to the orthorhombic structure.

The quadrupole frequency (or V_{zz}) for this structure is within errors similar to the one obtained with the one-site model. In contrast, the other hyperfine parameters η and δ are symmetric and narrow, respectively.

For $T \geqslant 373$ K the best fits show a unique hyperfine interaction in the tetragonal and cubic phases, respectively.

4.1.2. $Sr_{0.25}Ba_{0.75}HfO_3$. The analysis of the XRD pattern reveals that the structure of the powder sample is cubic at RT. At the vertices of this cubic cell there are 2 Sr and 6 Ba cations.

The time spectra for this composition were measured from RT to 1123 K. Best fits were obtained using a model consisting of only one static, asymmetric and disordered electric quadrupole hyperfine interaction.

In figure 3 the temperature dependence of the hyperfine parameters ω_Q, η and δ obtained from the fitted data are shown. The quadrupole frequency ω_Q does not present the decreasing temperature dependence observed in the previous compositions. It remains almost temperature independent with a mean value of 9.2 Mrads s^{-1}. The asymmetry parameter seems also to be constant, but the relative distribution width diminishes reversibly with temperature from 45% at RT to 15% at 525 K. Above this temperature δ also remains constant with a mean value of about 12%. Since in the whole temperature range there is no remarkable discontinuity in the quadrupole frequency or in the asymmetry parameter, it seems there is no structural phase transition.

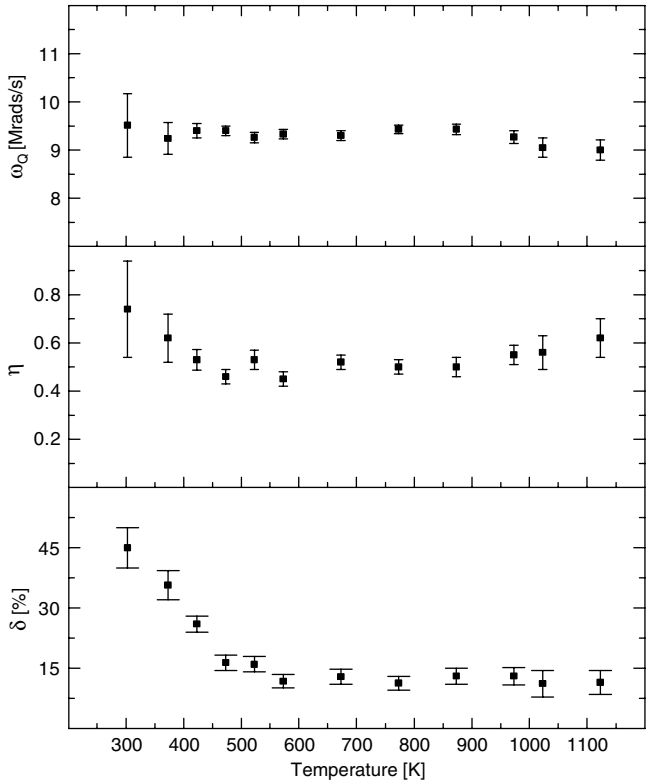

Figure 3. The temperature dependence of the hyperfine parameters in $Sr_{0.25}Ba_{0.75}HfO_3$.

Besides, the discontinuity in the relative line width at about 500 K cannot *a priori* be related to any structural phase transition. Probably it reflects a reversible ordering process in the distribution of Sr and Ba cations at the A-site.

4.1.3. $Sr_{0.12}Ba_{0.88}HfO_3$. The crystalline structure of this oxide is cubic at RT and in its unit cell vertices there are 7 Ba and 1 Sr cations. For this composition the PAC spectra were measured from RT to 1273 K. The hyperfine parameters were obtained by fitting a model consisting of a static, asymmetric and disordered electric quadrupole hyperfine interaction to the experimental data. In figure 4 the results of these fits are displayed. The quadrupole frequency ω_Q and the asymmetry parameter do not present any temperature dependence, with mean values of about 8.1 Mrads s^{-1} and 0.5, respectively. Similar to $Sr_{0.25}Ba_{0.75}HfO_3$, there is no remarkable discontinuity of the quadrupole frequency and the asymmetry parameter in the whole temperature range, indicating the absence of any structural phase transition.

The distribution width parameter diminishes reversibly with temperature from RT to 425 K. At RT δ is ∼80% and above ∼425 K it remains constant, with a mean value of ∼30%. This behaviour seems to be similar to what is observed for $x = 0.75$ but with higher δ values. In principle these results are inconsistent with a random distribution of cations because a smaller value for the line width parameter is expected as x goes to 0 or 1.

4.1.4. The behaviour of the hyperfine parameters in the cubic phase. At high temperatures, all compounds studied here have a cubic $Pm\bar{3}m$ structure. In perfect perovskites symmetry

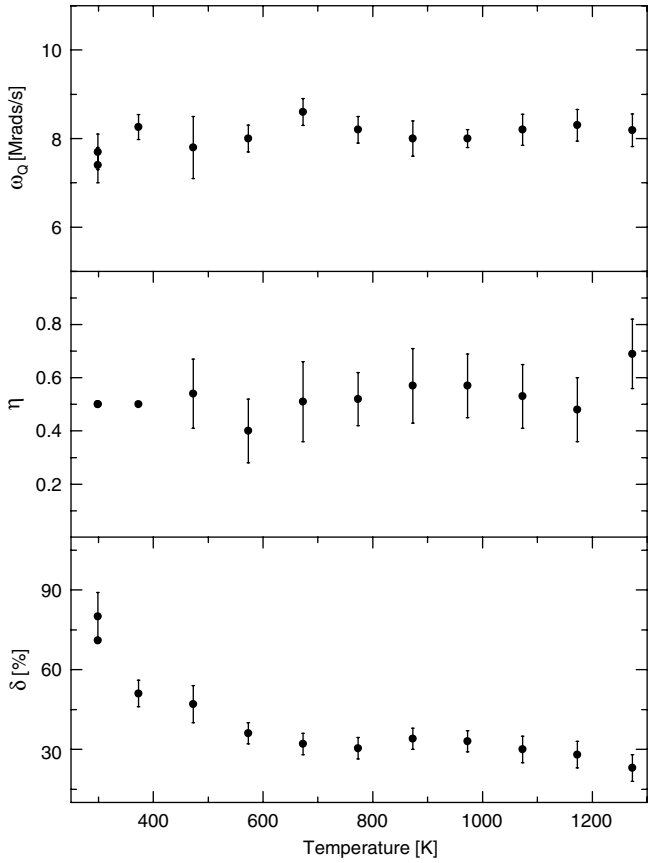

Figure 4. The temperature dependence of the hyperfine parameters in $Sr_{0.12}Ba_{0.88}HfO_3$ is shown.

considerations determine that at the M-site of the C-$Pm\bar{3}m$ phase the EFG must be zero. However, an asymmetric, disordered and weak electric quadrupole interaction was observed.

The EFG at Ta probes at M-sites in the cubic phase of the $Ba(TiHf)O_3$ family was studied. In this system the behaviour of V_{zz}, η and δ as the composition varies was simulated using the point charge model, and originated by random distributions of polarized oxygen vacancies and different charge states of the Ti and Hf cations. The charge of the oxygen vacancies was assumed to vary with M–O distances and produce non-zero EFG at the M-site. Similarly the different charges of M cations contribute to the EFG and the total effect reproduces $V_{zz}(x)$ reasonably well. The maximum of $V_{zz}(x)$ results from different charge states of M cations and the line width for intermediate compositions mostly by the polarized oxygen vacancies [4].

In figure 5 the hyperfine parameter dependence on composition measured at about 1300 K is shown. The quadrupole frequency (or V_{zz}) has a maximum value for $x = 0.50$, the asymmetry parameter is about 0.5 and independent of composition, and the line width has a maximum value for $x = 0.5$ and seems to be higher at extreme compositions.

The composition dependence of the hyperfine parameters in SBH is similar to that found in BTH. However, the maximum quadrupole frequency corresponding to BTH is about 80% higher than that found in SBH. This fact would indicate that the corresponding charge distributions are quite different. The asymmetry parameter in both cases is $\approx$0.5 and the line

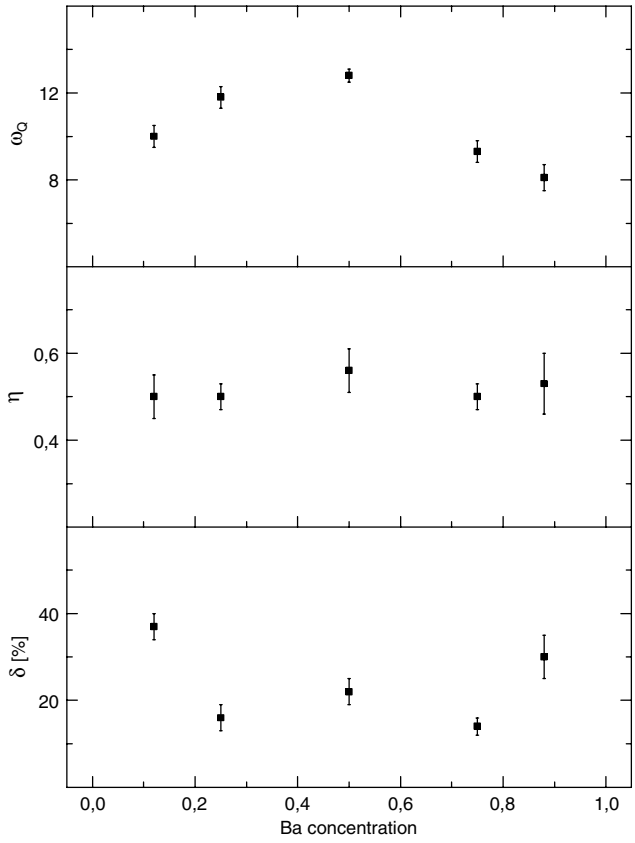

Figure 5. The hyperfine parameters corresponding to the SBH cubic phases.

width displays a maximum value for $x = 0.5$ and should tend to zero as statistical arguments predict for $x \rightarrow 0$ or 1. On the contrary, for these values of the composition, the line width seems to increase.

5. Discussion

The structural analysis of $Sr_{1-x}Ba_xHfO_3$ oxides at RT shows that the increase of Ba substitution at the Sr site produces a similar effect as temperature does in $SrHfO_3$.

In fact, as x varies from 0 to 1, the Sr–O and Ba–O bond competition produces an increase of the lattice constants that favours the formation of higher-symmetry structures at RT: orthorhombic → orthorhombic → tetragonal → cubic. The same effect was observed in $Sr_{1-x}Ba_xZrO_3$ (SBZ).

In contrast, for M-cation substitution as was observed in PZT and BTH there is not such correlation. At RT, the different structures of these compounds corresponding to different compositions do not coincide with the lattices of the pure oxides as temperature varies. Then it seems that the effect of A- and M-cation substitution have in common that they deform the unit cell by stretching (or squeezing) the lattice constants and producing different effects on the oxygen octahedron. In the first case it keeps the oxygen octahedron with minimum deformation, rotating it about the crystal axes as a rigid unit. The second case includes the deformation of the oxygen octahedron and a relative displacement of the M cation.

Table 3. The value of $\langle d_{A-O}\rangle$, $\langle d_{A+O}\rangle$ and the type of bond for the different compositions. (Note: In the crystal system and space group column, the prefixes O, T and C stand for orthorhombic, tetragonal and cubic, respectively.)

Ba (%)	Crystal system and space group	$\langle d_{A-O}\rangle$ Å	$\langle d_{A+O}\rangle$ Å	Bond
0	O-$Pbnm$	2.878	2.82	Ionic
12	O-$Pbnm$	2.899	2.84	Ionic
25	O-$Cmcm$	2.907	2.86	Ionic
50	T-$I4/mcm$	2.924	2.90	Ionic/covalent
75	C-$Pm\bar{3}m$	2.939	2.95	Covalent
88	C-$Pm\bar{3}m$	2.946	2.97	Covalent
100	C-$Pm\bar{3}m$	2.949	2.99	Covalent

The competition between Sr–O and Ba–O bonds in the pseudo-cubic approximation can be quantitatively considered by taking into account the sums of the effective ionic radii of cations and oxygen and comparing them to the cation–oxygen distances deduced from the values of the lattice constants [19]. This analysis would allow the description of the electron distribution in the region between oxygen and A and M cations with coordination numbers 4, 12 and 6, respectively. In the A–O case, the effective ionic radius sums are $r_{Sr+O} = 2.82$ Å and $r_{Ba+O} = 2.99$ Å [20]. The mean effective radii sum for composition x can be calculated using $\langle d_{A+O}\rangle = x r_{Ba+O} + (1-x) r_{Sr+O}$ and the mean distance between the A cation and nearest oxygen ($\langle d_{A-O}\rangle$) can be deduced from the lattice constants $\langle \mathbf{a}\rangle$ shown in table 1. For real compounds with lower symmetries and consequently smaller coordination numbers, with shorter ionic radii and $\langle d_{A-O}\rangle$ distances the approximation of these structures by an equivalent pseudo-cubic lattice with its corresponding coordination numbers implies that the bonds have to be considered on average as ionic or covalent.

In $PbTiO_3$, the procedure to determine if a bond is ionic or covalent by comparing the sum of ionic radii of cations and oxygen with appropriated lattice distances was verified by an x-ray charge–density study on the bonding electron distributions associated with the orbital hybridization [19].

In table 3 the quantities $\langle d_{A-O}\rangle$ and $\langle d_{A+O}\rangle$ are displayed for the pseudo-cubic and cubic lattice, respectively. The mean distance $\langle d_{A-O}\rangle = \langle a\rangle/\sqrt{2}$ between the A cation and closest oxygen obtained from the pseudo-cubic lattice parameter for different compositions was calculated. From $x = 0.12$ and up to 0.88 an almost linear relation between $\langle d_{A-O}\rangle$ and the composition is observed, indicating a uniform stretching of the lattice as the number of Ba cations increases. However, in the Sr- and Ba-rich regions where the corresponding structures are similar to those of the pure oxides, the slope is steeper or less steep, respectively. These results show qualitatively that the effect of a few impurity atoms on $\langle d_{A-O}\rangle$ due to the competition of Sr–O and Ba–O bonds is more important in the Sr-rich than in Ba-rich region, indicating that the stretching of the lattice induced by one Ba ($x = 0.12$) cation is more significant than the squeezing led by one Sr ($x = 0.88$).

The A–O bonds in pure oxides of $SrHfO_3$ and $BaHfO_3$ are ionic and covalent, respectively. This last result is opposed to what is commonly accepted because the A–O bond is mostly considered ionic. Then as x goes from 0 to 1 in SBH the A–O bond transforms from ionic to covalent. When $x = 0.5$ this approximation cannot distinguish the character of the bond.

A similar analysis of the M–O bonds was done. The sum of the effective ionic radius of Hf^{4+} and O^{2-} ($\langle d_{Hf+O}\rangle = 2.06$ Å) with coordination numbers of 6 and 2, respectively, as compared with the distances $\langle d_{Hf-O}\rangle = \langle a\rangle/2$ for $0 \leqslant x \leqslant 1$ reveals that the Hf–O bond is covalent if $x < 0.50$, undefined for $x = 0.5$ and ionic for higher compositions.

These simple approximations allow us to infer the following about the electron distribution in the oxygen–cation bond in $Sr_{1-x}Ba_xHfO_3$ perovskites: when the A–O bond is ionic the M–O bond is covalent and vice versa. The competition between Sr–O and Ba–O bonds seems to determine the nature of the Hf–O bond.

How do these approximations influence the analysis of data provided by the hyperfine interaction? In SH the Sr–O bond is ionic and the Hf–O is covalent. For a composition $x = 0.12$ and at RT the crystalline structure of this compound and SH are similar, the volume of the solid solution is 2% bigger and the components of the EFG tensor have increased uniformly by about 27%. The Sr–O bond favours the reduction of the lattice constant, in contrast to the Ba–O bond that favours the stretching. Thus the ionic Ba–O bond is more repulsive than the ionic Sr–O bond. In equilibrium a mean A–O distance would result and probably charge redistribution would also occur. These effects would mainly reflect an extra repulsion of 2p oxygen electrons caused by the extra 6s barium electrons added to the cubic cell. Calculations of the EFG in the perovskite M-site using state of the art methods, as for example the WIEN2K code, show that mostly O p and M d hybridized states produce the maximum contribution to the quadrupole interaction [21]. Then the presence of Ba in one of the cube vertices would induce charge redistribution that is reflected in the hybridized p–d state of the M–O bond, probably increasing the density of p electrons contribution at the M-site.

On doubling the number of Ba cations in the pseudo-cubic unit cell, the diffraction data show that the competition between Sr–O and Ba–O produces similar effects as for $x = 0.12$, i.e. the stretching of the unit cell. However, it does not produce any effect on the hyperfine parameters because their values for $x = 0.25$ are quasi-identical to those corresponding to the first composition. Thus although A–O and M–O distances increase reducing the EFG, this effect is compensated by a charge redistribution and a saturation effect seems to be observed.

In the $x = 0.5$ composition on average there are an equal number of Sr and Ba cations in the cubic unit cell. The stretching process of the lattice constant continues, barium almost enters in contact with oxygen and this simple model cannot distinguish if the bond is ionic or covalent. This same situation is also observed for the M–O bond. Thus the lattice expansion and the charge redistribution in the M–O bond would produce the reduction of the EFG.

For Ba-rich compositions the effect proposed for $x = 0.5$ continues and the reduction of the EFG is produced because the M–O distance increases and the charge distribution tends to have cubic symmetry.

The asymmetry parameter seems to be independent of composition with a value close to 0.5 [22]. It is not possible to explain this result because the actual charge distribution is unknown unless precise estimations based in *ab initio* electron density calculations are performed.

No reason exists to explain the increase of the relative line width as the Ba concentration tends to 1. Moreover in BH a relaxation process instead of a static, asymmetric and disordered quadrupole interaction can be fitted to the data. Thus as $x \rightarrow 1$ the disorder in the charge distribution increases and when x is 1 a time-relaxing process seems to appear [23].

6. Conclusions

In this work the structure and the hyperfine interactions as a function of temperature in the $Sr_xBa_{1-x}HfO_3$ family for $x = 0.12, 0.25, 0.50, 0.75$ and 0.88 were determined. The correlation between structures at RT of SH and SBH has been verified. Using classic parameters such as ionic radii, simple ideas of ionic and covalent bonds allowed the interpretation of the data. As x goes from 0 to 1, ionic to covalent bond transition and covalent to ionic bond transition in A–O and M–O interactions, respectively, are proposed. The concentration

dependence of the EFG in terms of lattice expansion and charge transfer form A–O to M–O bonds is also proposed.

References

[1] Kennedy B J, Howard C J, Thorogood G J and Hester J R 2001 *J. Solid State Chem.* **161** 106
[2] Noheda B, Cox D E, Shirane G, Gonzalo J A, Cross L E and Park S-E 1999 *Appl. Phys. Lett.* **74** 2059
[3] Payne W H and Tennery V J 1965 *J. Am. Ceram. Soc.* **48** 413
[4] Alonso R E, Ayala A P, de la Presa P, Horowitz C and López-García A 2002 *Ferroelectrics* **274** 17
[5] Kennedy B J, Howard C and Chakoumakos B C 1999 *Phys. Rev.* B **59** 4023
[6] López-García A, de la Presa P and Ayala A 2001 *J. Solid State Chem.* **159** 1
[7] López-García A, de la Presa P, Rodríguez A M, Saitovich H and Silva P R J 1993 *Phys. Rev.* B **47** 84
[8] Sebastian K C, Somayajulu D R S, Jaffrey S N A, Sharma S S and Varma J 1996 *Hyperfine Interact.* **99** 347
[9] Frauenfelder H and Steffen R M 1968 *Alpha-, Beta- and Gamma-Ray Spectroscopy* ed K Siegbahn (Amsterdam: North-Holland) p 997
[10] Butz T and Lerf A 1983 *Phys. Lett.* A **97** 217
[11] Stoneham A M 1969 *Rev. Mod. Phys.* **41** 82
[12] Horowitz C, Alonso R E, López-García A, Lamas D G and Caneiro A 2002 *Ferroelectrics* **269** 117
[13] Alonso R E, Horowitz C and López-García A 2001 *Hyperfine Interact.* **136/137** 541
[14] Rao C N and Rao K J 1978 *Phase Transitions in Solids* (New York: McGraw-Hill)
[15] Catchen G L, Hollinger E F and Rearick T M 1996 *Z. Naturf.* a **51** 411
[16] Dogra R, Junqueira A C, Saxena R N, Carbonari A W, Mestnik-Filho J and Moralles M 2001 *Phys. Rev.* B **63** 4104
[17] Kennedy B J, Li L, Garret R F, Kubota Y and Kato K 2002 *Solid State Commun.* **122** 355
[18] Alonso R E, Horowitz C, López-García A, Lamas D G and Caneiro A 2001 *Solid State Commun.* **120** 205
[19] Kuroiwa Y, Aoyagi S, Sawada A, Harada J, Nishibori E, Takata M and Sakata M 2001 *Phys. Rev. Lett.* **87** 217601
[20] Shannon R D 1976 *Acta Crystallogr.* A **32** 751
[21] Blaha P, Schwarz K, Madsen G H K, Kvsnicka D and Luitz J 2001 *WIEN2k* Karlheinz Schwarz Technical University, Vienna, Austria
Schwarz K, Blaha P and Madsen G H K 2002 *Comput. Phys. Commun.* **147** 71
[22] Ayala A P and López-García A 1999 *Hyperfine Interact.* **120/121** 163
[23] López-García A, de la Presa P, Rodríguez A M, Saitovich H and da Silva P R J 1993 *Phys. Rev.* B **47** 84